Available online at www.sciencedirect.com
ScienceDirect
Journal of Power Sources 167 (2007) 272–280
JOURNAL OF POWER SOURCES
www.elsevier.com/locate/jpowsour

Pt and PtRu nanoparticles deposited on single-wall carbon nanotubes for methanol electro-oxidation

Zhaolin Liu [a,*], Xing Yi Ling [a], Bing Guo [a], Liang Hong [a,b], Jim Yang Lee [a,b]

[a] *Institute of Materials Research & Engineering, 3 Research Link, Singapore 117602, Singapore*
[b] *Department of Chemical and Environmental Engineering, National University of Singapore, 10 Kent Ridge Crescent, Singapore 119260, Singapore*

Received 29 January 2007; accepted 14 February 2007
Available online 27 February 2007

Abstract

Platinum (Pt) and platinum–ruthenium (PtRu) nanoparticles supported on Vulcan XC-72 carbon and single-wall carbon nanotubes (SWCNT) are prepared by a microwave-assisted polyol process. The catalysts are characterized by transmission electron microscopy (TEM), X-ray diffraction (XRD) and X-ray photoelectron spectroscopy (XPS). The PtRu nanoparticles, which are uniformly dispersed on carbon, have diameters of 2–6 nm. All the PtRu/C catalysts display the characteristic diffraction peaks of a face centred cubic Pt structure, excepting that the 2θ values are shifted to slightly higher values. The results from XPS analysis reveal that the catalysts contain mostly Pt(0) and Ru(0), with traces of Pt(II), Pt(IV) and Ru(IV). The electrooxidation of methanol is studied by cyclic voltammetry, linear sweep voltammetry, and chronoamperometry. Both PtRu/C catalysts have high and more durable electrocatalytic activities for methanol oxidation than a comparative Pt/C catalyst. Preliminary data from a single direct methanol fuel cell using the SWCNT supported PtRu alloy as the anode catalyst delivers high power density.

Keywords: Methanol electro-oxidation; Single-wall carbon nanotubes; Fuel cell; Power density; Platinum catalyst; Platinum–ruthenium nanoparticle

1. Introduction

Direct methanol fuel cells (DMFCs) are prospective power sources for portable electronic devices. Challenging issues such as methanol crossover and poor methanol electrooxidation kinetics are the main obstacles to the commercialization of DMFC technology [1–5]. Methanol crossover is the diffusion-driven phenomenon of methanol travelling through the membrane from the anode to the cathode. It affects the performance of the cathode and lowers the efficiency of a DMFC. The other issue is the slow electrochemical reaction of the DMFC. Previous research has led to the conclusion that the choice and preparation of the anode catalyst in a DMFC is far more important than in other types of fuel cell. This is because the kinetics of methanol electro-oxidation are relatively slow, namely, about six orders of magnitude lower than those of hydrogen near room temperature. Therefore, if the anode catalyst is of poor quality, a DMFC may not even operate.

At present, PtRu particles supported on carbon are the most promising catalyst material for DMFC anodes. Alloy catalysts of high surface area are generally prepared by co-impregnation [6], co-precipitation [7], absorbing alloy colloids [8–10] or surface organometallic chemistry techniques [11,12]. The activity of these multi-component catalysts has been shown to depend strongly on the preparation conditions [13]. While activated carbon is still the most common support material for electrocatalysts, new forms of carbon such as fullerenes and nanotubes, which have become more available recently, have also been investigated as catalyst supports. The deposition of Pt, Ru and PtRu on graphite nanofibres, multi-walled carbon nanotubes (MWCNT), single-walled carbon nanotubes (SWCNT) and carbon nanocoil have been reported [14–23] and the resulting supported catalysts have been found to be superior to those using an activated carbon support.

We have proposed a new method of preparing carbon supported Pt and PtRu catalysts which are active towards methanol electro-oxidation at room temperature [10], as part of our continuing work on developing low-cost processes for the preparation of homogenous and well-defined nanoparticle catalysts for fuel cell applications. In the present work, thiol-encapsulated Pt and

* Corresponding author. Tel.: +65 68727532; fax: +65 68720785.
E-mail address: zl-liu@imre.a-star.edu.sg (Z. Liu).

0378-7753/$ – see front matter © 2007 Elsevier B.V. All rights reserved.
doi:10.1016/j.jpowsour.2007.02.044

PtRu colloids are synthesized, deposited on SWCNT, and then heat-treated to produce SWCNT supported Pt and PtRu catalysts. The crystal structure and electrochemical activity for methanol electro-oxidation of the resulting catalysts is investigated.

2. Experimental

2.1. Colloid synthesis

Analytical grades of hydrogen hexachloroplatinate hydrate, ruthenium chloride, sodium hydroxide, ethylene glycol, toluene, and 1-dodecanethiol (DDT) were used for colloid synthesis. All aqueous solutions were prepared with distilled, de-ionized water.

A 2 ml sample of aqueous 20 mM hydrogen hexachloroplatinate hydrate solution was mixed with 25 ml of ethylene glycol to produce a yellowish solution. The solution was placed in a CEM microwave reactor for 60 s with the maximum temperature set at 170 °C. On heating, the solution changed colour from yellow to yellowish brown, and was then left to cool to room temperature naturally. The cooled mixture was diluted with 1–2 times its volume of distilled, de-ionized water. The diluted Pt colloid solution was added to 25 ml of a toluene solution of 1-dodecanethiol to provide a thiol:Pt molar ratio in the range of 3–10. The bi-phasic mixture was vigorously stirred for a few minutes during which the transfer of Pt from the ethylene glycol/water phase to toluene occurred to leave a clear aqueous solution. The synthesis of the binary PtRu nanoparticles was carried out similarly, using 2 ml of 20 mM of H_2PtCl_6, 2.5 ml of 20 mM $RuCl_3$, and 25 ml of ethylene glycol in the starting mixture. EXD analysis showed that the atomic Pt:Ru ratio in the bimetallic colloid was 52:48.

2.2. Preparation of catalysts

The stable thiol-encapsulated Pt and PtRu colloids were supported on high-surface-area Vulcan XC-72 carbon and SMCNT (as-synthesized Pt and as-synthesized PtRu colloid catalysts, 20 wt.% metal content) by combining a toluene dispersion of Pt or PtRu colloid with a suspension of Vulcan carbon or SWCNT in toluene. The solution was stirred vigorously for 2 h. Solvent was evaporated and the solid residue was rinsed with ethanol. Finally, the powder was dried at 60 °C in vacuum.

In order to remove the stabilizing shell on the nanoparticles, as-synthesized Pt and PtRu colloid catalysts were heat treated for 5 h in argon at 360 °C. The furnace was purged with argon gas for at least 15 min prior to the heat treatment. All prepared catalysts had a nominal metal loading of 20 wt.% on the Vulcan carbon black or SWCNT support. The samples are identified as heat-treated Pt and heat-treated PtRu catalysts in the following discussion.

2.3. Characterization

The Pt or PtRu colloidal formation process was monitored by UV–vis spectroscopy on a Shimadzu UV-2501 PC double beam spectrophotometer in the region of 220–800 nm, using 1 cm path length quartz cuvettes. The particle morphology, size, and size-distribution of the colloids and catalysts were characterized by transmission electron microscopy (TEM) using a Philips CM300 FEG system operating at 300 kV. The TEM samples were prepared by placing a drop of the colloidal dispersion or a sonicated (1 h) catalyst suspension in acetone on a 3 mm Cu grid, following by drying under ambient conditions. Fourier transform infrared (FT-IR) spectra were taken from films drop-cast from the colloidal solutions on to KBr salt plates, using a Perkin-Elmer Spectrum 2000 FT-IR spectrometer at 1 cm^{-1} resolution. X-ray photoelectron spectroscopic (XPS) analysis was carried out with a VG ESCALAB MKII instrument that used a Mg Kα X-ray source. The XPS samples were prepared by dispensing the colloidal solution on to a polished graphite surface followed by drying.

2.4. Electrochemical measurements

An EG&G Model 273 potentiostat/galvanostat and a conventional three-electrode test cell were used for electrochemical measurements. The working electrode was a thin layer of Nafion-impregnated catalyst cast on a vitreous carbon disc held in a Teflon cylinder. The catalyst layer was obtained as follows: (i) a slurry was first prepared by sonicating for 1 h a mixture of 0.5 ml of de-ionized water, 0.06 g of Pt/C or PtRu/C catalyst, and 0.5 ml of Nafion solution (Aldrich: 5 wt.% Nafion); (ii) 7 μl of the slurry was pipetted and spread on the carbon disc; (iii) the electrode was dried at 90 °C for 1 h and mounted on a stainless-steel support. The surface area of the vitreous carbon disc was 0.25 cm^2. A Pt gauze and a Ag/AgCl electrode were used as the counter and reference electrodes, respectively. All potentials are reported with respect to the Ag/AgCl electrode. All electrolyte solutions were purged with high-purity argon for 2 h prior to each measurement. For cyclic voltammetry of methanol oxidation, the electrolyte solution was 2 M CH_3OH in 1 M H_2SO_4 and was prepared from high-purity sulfuric acid, high-purity methanol, and distilled water.

The membrane electrode assembly (MEA) for the DMFC test cell was made by hot-pressing pretreated Nafion® 1135 together with an anode sheet and a cathode sheet. The anode sheet was a carbon paper (SGL, Germany) with SWCNT and a Vulcan carbon supported Pt or PtRu catalyst layer. The cathode sheet was a carbon paper with a carbon-supported 40 wt.% Pt catalyst layer supplied by E-TEK. The catalyst loadings at the anode and cathode were 4 and 3 mg cm^{-2}, respectively, and the effective electrode area was 6 cm^2. The fuel was 2 M CH_3OH delivered at 2 ml min^{-1} by a micropump. The oxygen flow was regulated by a flowmeter at 500 cm^3 min^{-1}.

3. Results and discussion

3.1. Physicochemical characterization of as-synthesized Pt or PtRu colloid and heat-treated Pt or PtRu/SWCNT catalysts

The formation of Pt colloids via microwave dielectric heating was followed by UV–vis spectroscopy. The H_2PtCl_6 solution before microwave irradiation is pale yellow and shows a peak at

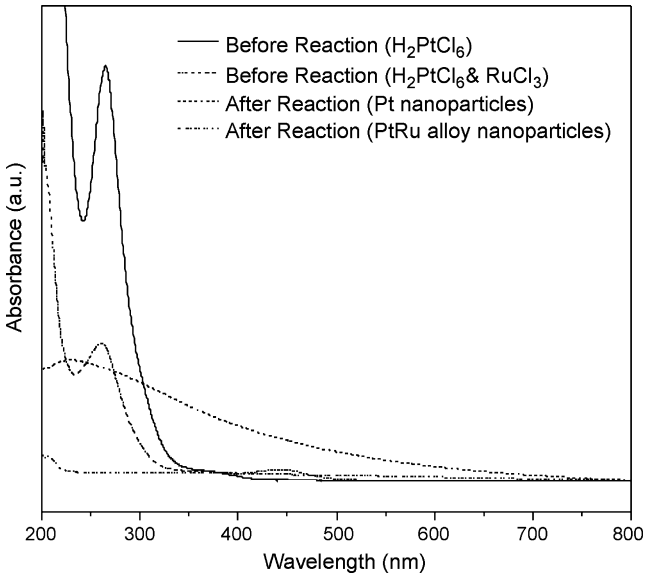

Fig. 1. UV–vis absorption spectra of solution containing H_2PtCl_6 and a mixture of H_2PtCl_6 and $RuCl_3$ before and after microwave irradiation.

260 nm in its UV–vis spectrum (Fig. 1) as a result of the ligand-to-metal charge-transfer transition in the $PtCl_6^{2-}$ ion [24,25]. The colour of the solution changes to dark brown after the reaction. The peak at 260 nm is no longer visible, which suggests that all the $PtCl_6^{2-}$ ions are completely reduced. The spectrum of the completely reduced solution displays strong absorption from 700 nm and a gradually increasing intensity from the visible to the ultraviolet region. These features confirm the formation of colloids [26]. When the Pt colloid in ethylene glycol is diluted with distilled de-ionized water and mixed with a toluene solution of DDT, transfer of Pt from the ethylene glycol–water phase to toluene takes place. This is visually evident from the colour change in the two phases. The colour of the ethylene glycol and water solution fades gradually to colourless, whereas the colour of the toluene and hexane phase darkens from colourless to yellowish brown or dark brown.

It was found that the addition of NaOH to $RuCl_3$ (or a mixture of H_2PtCl_6 and $RuCl_3$) resulted in an instant color change from dark brown to yellow–green, due to the formation of ruthenium hydroxide complexes. This was also shown spectroscopically by the evolution of a peak at ∼436 nm. The observation is similar to that of Pârvulescu [27]. On the formation of PtRu alloy nanoparticles, the characteristic absorptions of Ru^{3+} and $PtCl_6^{2-}$ ions at 436 and 260 nm disappear and are replaced by gradually decreasing absorption from the ultraviolet region to 700 nm, which indicates the formation of PtRu nanoparticles.

The particle size formed under different conditions is shown in Table 1. Nearly monodispersed and spherical particles are produced in all Pt colloidal solutions. Six different pH precursors are tested; they range from 1.44 to 10.46. When the precursor solution is adjusted to a pH of 1.44, the resulting nanoparticles grow to 7.40 ± 0.88 nm, which is attributed to a domination of particle growth during the reduction process as a result of an inadequate number of repulsive OH^- ions in solution. Within the pH buffer range of 1.65–5.56, pH changes in the precursors have no significant impact on the size of the nanoparticles. On the other hand, smaller nanoparticles are formed (size ∼1.92 nm) at a pH of 10.46. In summary, the addition of a large amount of NaOH to the precursor accelerates the formation of large number of nuclei and particle growth is significantly retarded because of the strong electrostatic repulsion of OH^- ions.

Nanoparticles synthesized by two different irradiation heating times, i.e., 30 and 90 s, were compared. With a time difference, of only 60 s, there is a great different in terms of particle size, namely, 4.70 and 6.10 nm, due to the extent of nucleation and growth. Yet both samples have maintained a very narrow size-distribution (0.40 and 0.54 nm, respectively) due to homogeneous microwave dielectric heating. This result is understandable as the rate of reaction with microwave dielectric heating can be at least 2–3 times faster than that with the conventional conductive-dominant reflux method [28].

Unlike conventional chemical reductions, the shape and size of the Pt nanoparticles synthesized by microwave dielectric heating are not sensitive to the amount of DDT present in toluene.

Table 1
Pt colloids prepared by microwave irradiation heating under different conditions

Conditions	pH before reaction	pH after reaction	Irradiation time (s)	Concentration of precursor (mM)	DDT/Pt ratio	Average diameter (nm)	Standard deviation (nm)
pH effect	1.44	0.9	30	1	100	7.40	0.88
	1.65	0.91				4.70	0.40
	2.02	1.26				4.88	0.63
	5.56	1.24				4.77	0.57
	9.45	1.35				3.55	0.39
	10.46	1.5				1.92	0.40
DDT/Pt ratio	1.65	0.91	30	1	3	4.68	0.38
					100	4.70	0.40
Concentration of precursor	1.65	0.91	30	0.5	100	2.97	0.43
				1		4.70	0.40
				3		5.81	0.44
				5		6.75	0.66
Irradiation time (s)	1.65	0.91	30	1	100	4.70	0.40
			90			6.10	0.54

For example, a comparison of Pt nanoparticles for a DDT-to-Pt ratio of 3 and 100 shows no significant changes in the size or the size distribution (Table 1). This implies that DDT serves as a good stabilizing agent against particle agglomeration and as a capping agent for the transfer of Pt from ethylene glycol to the toluene solution. This is a result of the strong affinity of the sulfur group in DDT for the Pt surface.

Nanoparticles with sizes in the range 3–6.75 nm are obtained when the concentration of the precursor is increased from 0.5 to 5 mM (Table 1). The increase in the metal salt concentration increases the frequency of intermolecular collisions and thereby provides a greater opportunity for the formation of nuclei. These small nuclei will then continue to form large clusters via a coalescence process. Typical TEM images of the Pt and PtRu colloids are presented in Fig. 2(a) and (b), respectively, and show a remarkably uniform and high dispersion of the metal and the alloy particles. The average diameters of 4.7 nm (for Pt) and 4.5 nm (for PtRu) are accompanied by relatively narrow particle-size distributions (Fig. 2(c) and (d), range: 3–6 nm, standard deviations = 0.4 nm). Adsorption of the colloidal particles on SWCNT followed by thermal treatment (in an argon gas at 360 °C for 5 h) to remove the stabilizing alkanethiol layer does not bring about significant changes in morphology (Fig. 3a and b). The Pt and alloy nanoparticles are in a state of high dispersion over the carbon surface, and the size of the particles remains virtually unchanged.

The FT-IR spectrum of the thiol-encapsulated platinum colloid is compared with that of pure decanethiol in Fig. 4. The two strong peaks at 2924 and 2852 cm^{-1}, which correspond to the antisymmetric (d^-) and symmetric CH_2 (d^+) stretches, are ~5 cm^{-1} higher than the literature values [29]. These peaks have been assigned to highly ordered alkyl chains surrounding a platinum core, and may be used to indicate the attachment of thiol to the platinum surface. This spectral feature is not observed in the pure thiol spectrum because of the random orientation of the alkyl group.

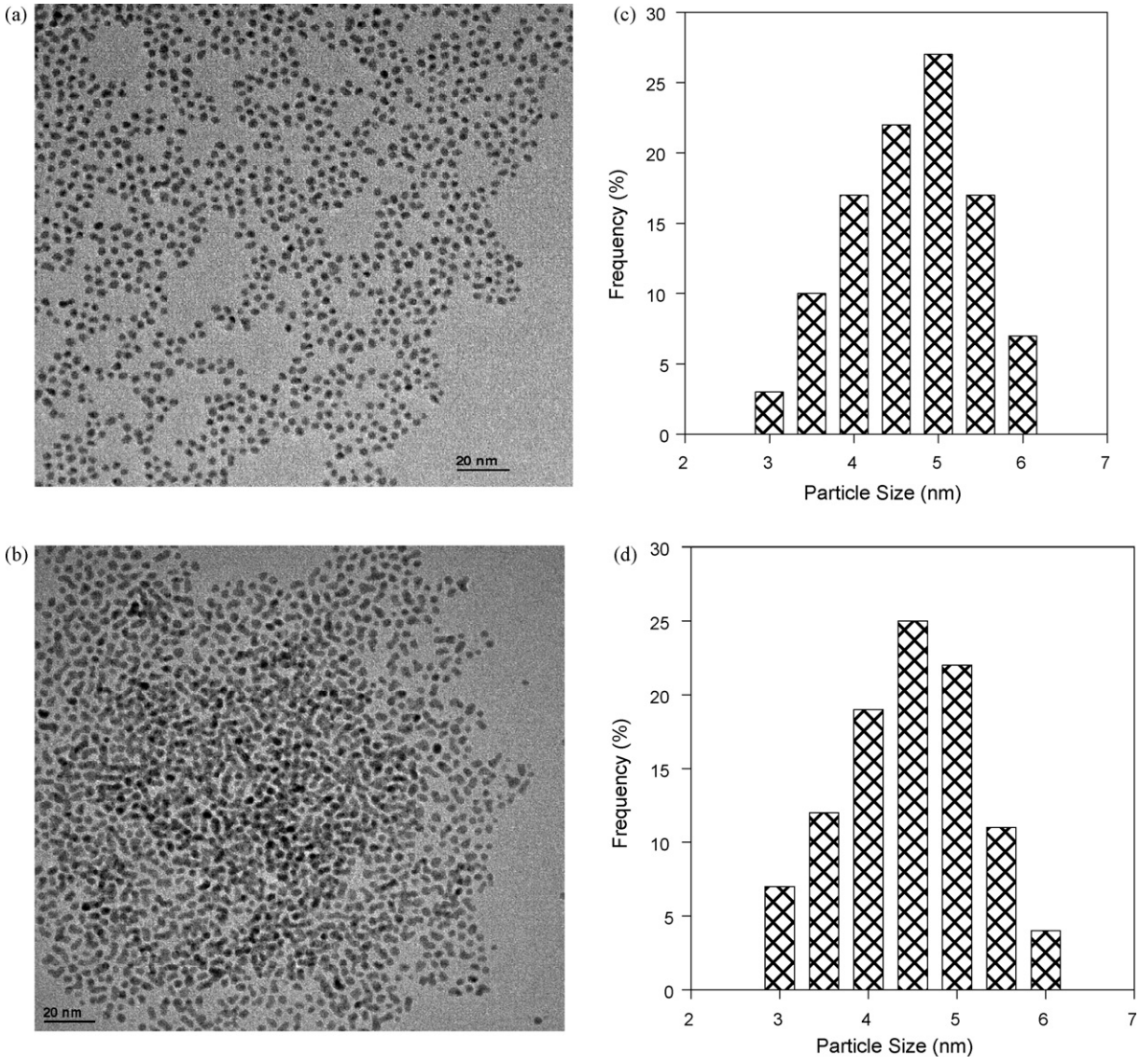

Fig. 2. Transmission electron micrographs of (a) as-synthesized Pt and (b) PtRu colloid catalysts. Histograms of particle-size distributions for as-synthesized (c) Pt and (d) PtRu colloids.

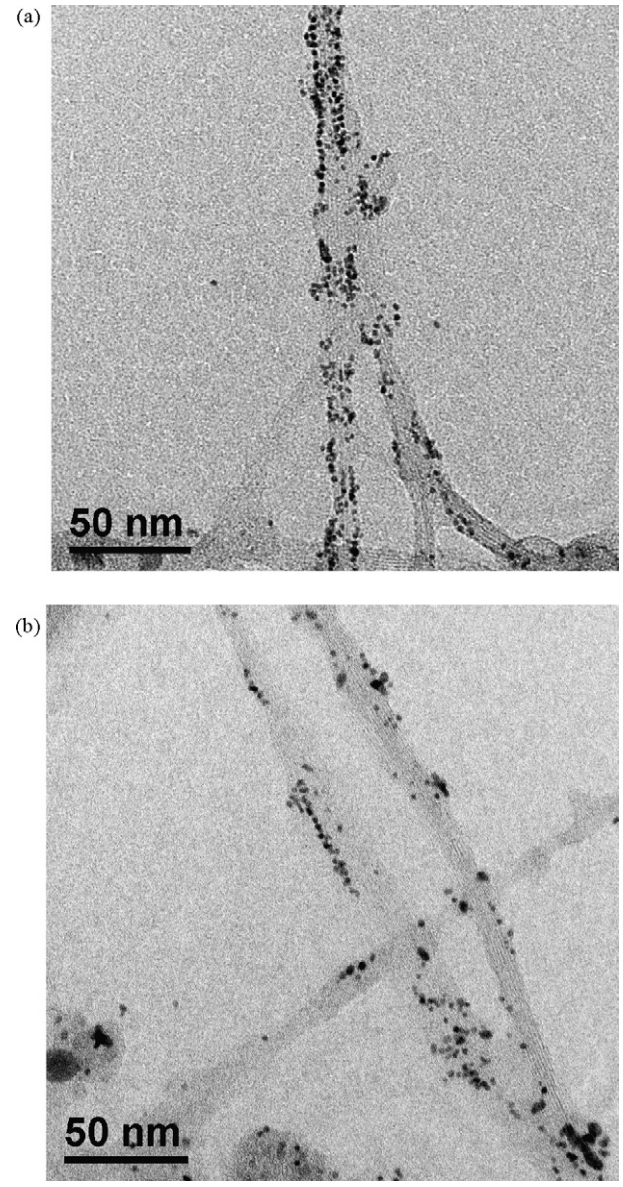

Fig. 3. Transmission electron micrographs of (a) Pt/SWCNT and (b) PtRu/SWCNT catalysts.

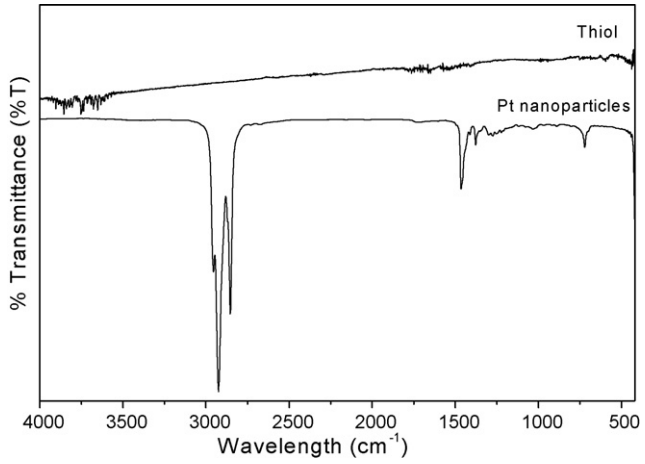

Fig. 4. Infrared spectra of DDT-encapsulated Pt nanoparticles.

The surface composition and chemical states of the stabilized colloids were examined by XPS. The narrow-scan spectra in the S 2p, Pt 4f and Ru 3p regions for DDT-encapsulated PtRu colloids are presented in Fig. 5. The S 2p region is characterized by a doublet between 158 and 168 eV that arises from spin-orbital coupling ($2p_{3/2}$ and $2p_{1/2}$). The $2p_{3/2}$ (162.9 eV) and $2p_{1/2}$ (164.0 eV) sub-bands in the sample under study are present in a ratio of 2:1, which is consistent with the literature value [30]. Free thiols often display a more intense $2p_{3/2}$ band at about 164.0 ± 1.18 eV. The binding energy (BE) for adsorbed thiol monolayers is lower, at ~162.9 eV, and is caused by strong attachment of the sulfur end of the thiol to the surface of the PtRu nanoparticle. This readily resolved spectral difference was used to identify the PtRu-bound sulfur species. The $2p_{1/2}$ signal at 164.0 eV was used to indicate the presence of unbounded –SH species from excess thiol [31].

The Pt 4f region shows two doublets from the spin-orbital splitting of the $4f_{7/2}$ and $4f_{5/2}$ states. Similar to the S 2p spectrum, the binding energies for Pt 4f are somewhat lower than the literature values because of the thiol attachment to the metal surface. The main doublet at 71.0 and 74.3 eV (in the peak area ratio of 4:3) is contributed by Pt $4f_{7/2}$, and can be used to indicate the presence of metallic platinum Pt(0). A smaller doublet due to Pt $4f_{5/2}$ is detected at 72.1 and 75.3 eV, which indicates the presence of higher oxidation states of Pt, such as Pt(IV) (e.g., PtO_2) in the sample. This is corroborated by the O 1s spectrum. The respective proportions of Pt(0) and Pt(IV) are 82% and 18%, respectively. The high Pt(0) content can be attributed to the inhibition of oxidation of metal colloids in non-aqueous solutions that are protected by surface-adsorbed glycol. As the binding energy for the Ru 3d line of zero-valent ruthenium at 284.3 eV [30] is very close to the C 1s line, which results from adventitious carbonaceous species, the Ru 3p spectrum is preferred for the analysis of the Ru oxidation state. The Ru $3p_{3/2}$ signal is deconvoluted into two distinguishable pairs of peaks of different intensities located at BE = 461.1 and 462.5 eV, which correspond well with Ru(0) and RuO_2, respectively [30]. The interaction between platinum and thiol can therefore be confirmed by combining the spectroscopic data obtained from the FT-IR and XPS studies.

3.2. Electrochemical performances

The real surface area of platinum for the Pt/SWCNT and PtRu/SWCNT catalysts (A_{EL}) is estimated from the integrated charge in the hydrogen absorption region (Q_H) of the cyclic voltammogram (hatched area in Fig. 6). The areas (in $m^2\,g^{-1}$) are calculated from the following formula assuming a correspondence value of 0.21 mC cm^{-2} (calculated from the surface density of 1.3×10^{15} atom cm^{-2}, a value generally taken for polycrystalline Pt electrodes [32]) and the Pt loading. Thus:

$$A_{EL}\,(m^2\,g^{-1}\ \text{catalyst}) = \frac{Q_H}{0.21 \times 10^{-3}\,C\,g\ \text{catalyst}} \quad (1)$$

As demonstrated by the results in Table 2, the Pt surface area is, as expected, lower in the supported PtRu catalysts. All measurements are made with almost the same catalyst loading on a

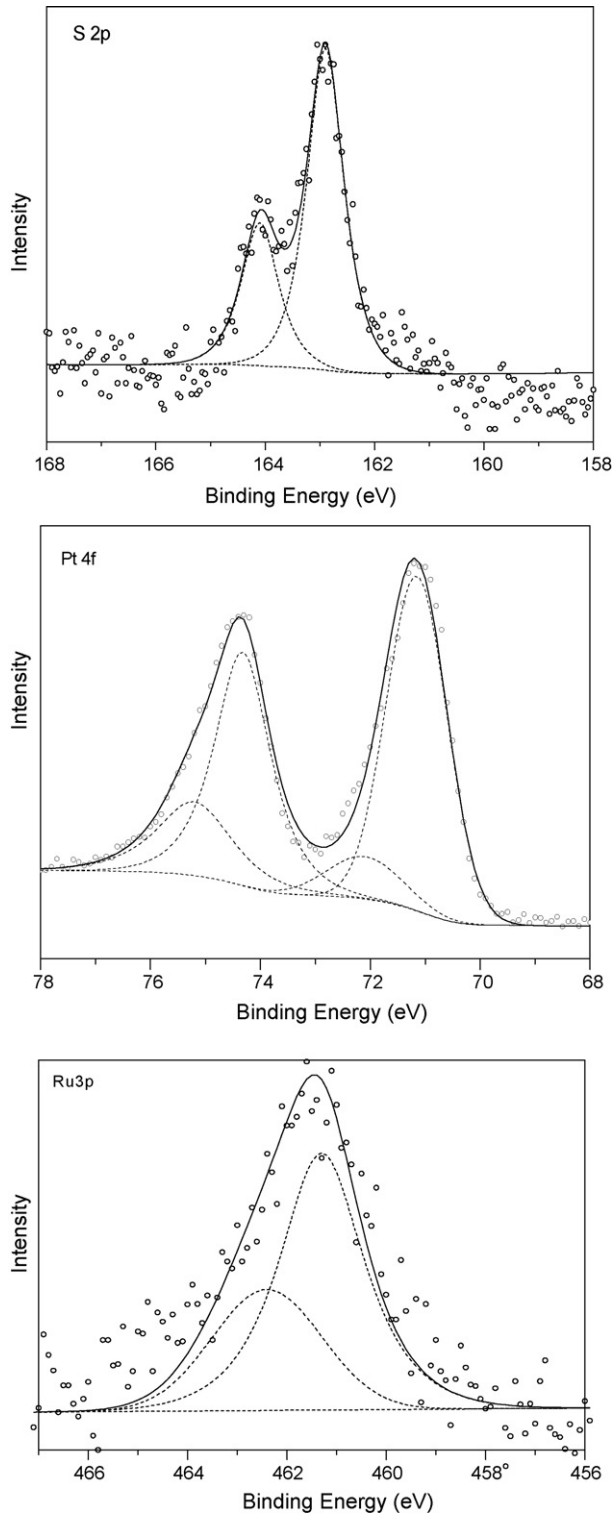

Fig. 5. X-ray photoelectron spectra of as-prepared PtRu colloids in S 2p, Pt 4f and Ru 3p region.

0.25 cm^2 disc electrode. If it is assumed that each noble metal retains its bulk properties, Ru will not chemisorb hydrogen above 0.2 V (NHE) while Pt will adsorb hydrogen strongly [33]. The addition of Ru therefore appears to have caused the platinum surface sites to be partially covered. Therefore, the PtRu/SWCNT has a lower real surface area than Pt/SWCNT. The use of Vulcan carbon or CNT does not cause significant differences in the Pt surface area. This is not surprising in view of the similarly small particle size of the metals in these supported bimetallic systems.

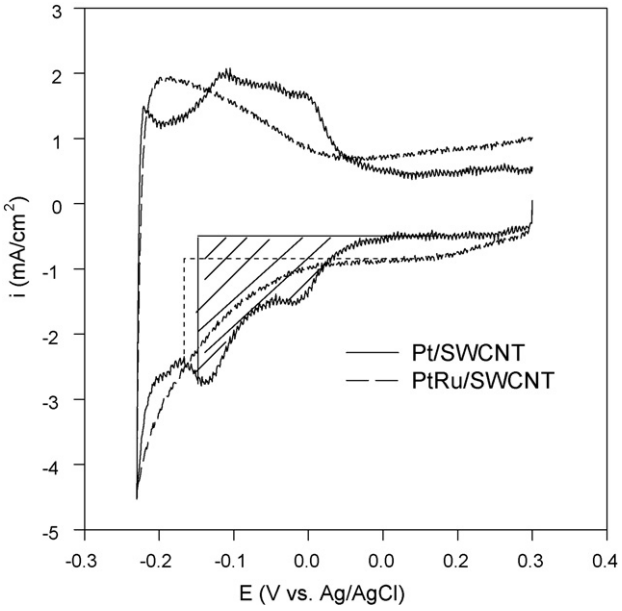

Fig. 6. Hydrogen electrosorption voltammetric profiles for Pt/SWCNT and PtRu/SWCNT catalysts in 1 M H_2SO_4 at a scan rate of 50 mV s^{-1} at room temperature. Hatched area represents amount of charge of electrosorption of hydrogen on Pt.

The Pt and PtRu alloy nanoparticles were characterized by cyclic voltammetry (CV) in an electrolyte of 1 M H_2SO_4/2 M CH_3OH (Fig. 7). The alloying effect due to ruthenium (in PtRu/Vulcan carbon and PtRu/SWCNT) is demonstrated by a lower onset potential for methanol electro-oxidation. The onset

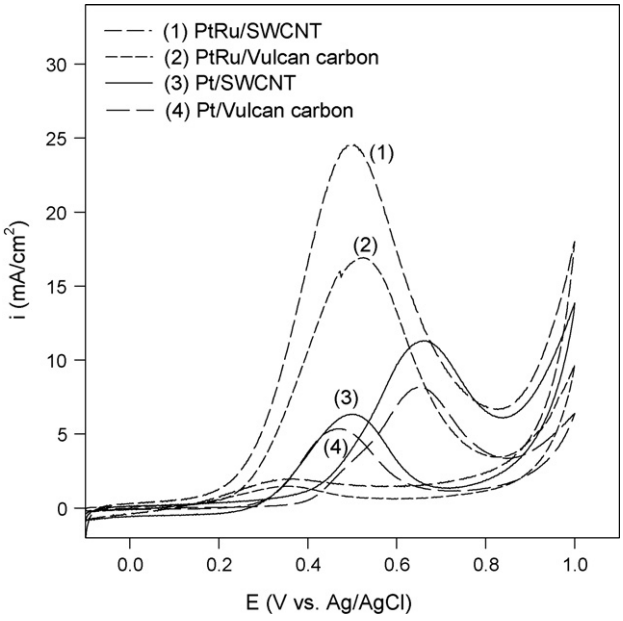

Fig. 7. Cyclic voltammograms of room temperature methanol electro-oxidation on different catalysts in 1 M H_2SO_4, 2 M CH_3OH at a scan rate of 10 mV s^{-1} at room temperature.

Table 2
Real (active) surface areas of Pt/SWCNT and PtRu/SWCNT catalysts as determined by hydrogen electro-adsorption

Origin of PtRu/C catalyst	Q_H[a] (mC)	S_{EL}[b] (cm^2)	Catalyst loading (mg 0.25 cm^{-2})	A_{EL}[c] ($m^2\ g^{-1}$ catalyst)	Onset potential (V)
Pt/Vulcan carbon	10.8	51.4	0.42	12.2	0.35
Pt/SWCNT	11.4	54.3	0.42	12.9	0.31
PtRu/Vulcan carbon	8.2	39.1	0.42	9.3	0.20
PtRu/SWCNT	8.5	40.5	0.42	9.6	0.19

[a] Q_H: charges exchanged during the electroadsorption of hydrogen on Pt or PtRu.
[b] S_{EL}: real surface area obtained electrochemically.
[c] A_{EL}: real surface area obtained electrochemically per gram of catalyst.

potential for PtRu/SWCNT is slightly lower (0.19 V) than that for PtRu/Vulcan carbon (0.20 V). During methanol oxidation experiments, a current density above the background level is detected as early as 0.1 V, and begins to escalate rapidly at 0.2 V (Fig. 7). This may be interpreted in terms of a water discharge reaction producing OH species that are chemisorbed on the Ru sites. The water discharge reaction on Ru sites and the formation of surface Ru–OH groups are kinetically more favourable than those on the Pt sites. It is generally believed that the Pt sites in a Pt–Ru alloy are involved in the methanol de-hydrogenation step and the strong chemisorption of the methanolic residues. At 0.2 V, the water discharge reaction occurs mostly on the Ru sites of the catalyst surface. The final step is the reaction between Ru–OH groups and neighbouring methanolic residues on Pt to yield carbon dioxide. Methanol oxidation is represented by the anodic peak at around 0.7 V for Pt/Vulcan carbon or SWCNT and 0.6 V for PtRu/Vulcan carbon or SWCNT. In the reverse scan, the adsorbed intermediates produce a second oxidation peak at 0.5 V for Pt/Vulcan carbon or SWCNT and 0.35 V for PtRu/Vulcan carbon or SWCNT. Comparative tests also show that Pt/SWCNT and PtRu/SWCNT are more active than Pt/Vulcan carbon and PtRu/Vulcan carbon, respectively.

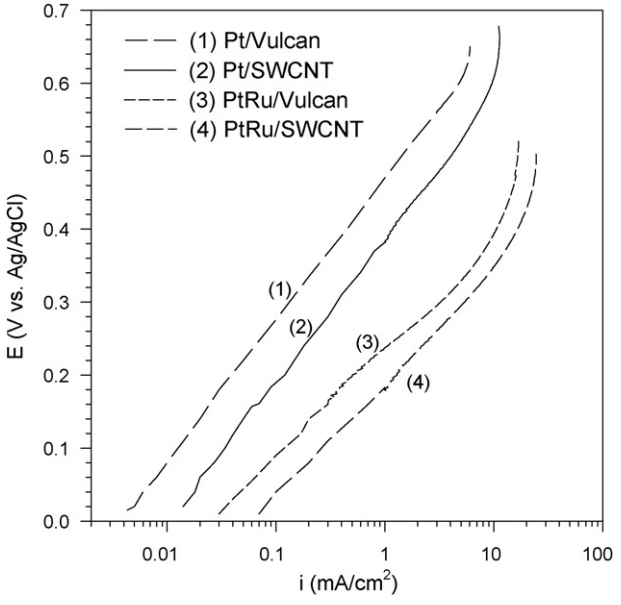

Fig. 8. Comparison of Tafel plot for methanol electro-oxidation on Pt/SWCNT or Vulcan carbon and PtRu/SWCNT or Vulcan carbon catalysts; 1 M H_2SO_4, 2 M CH_3OH at a scan rate of 10 mV s^{-1} at room temperature.

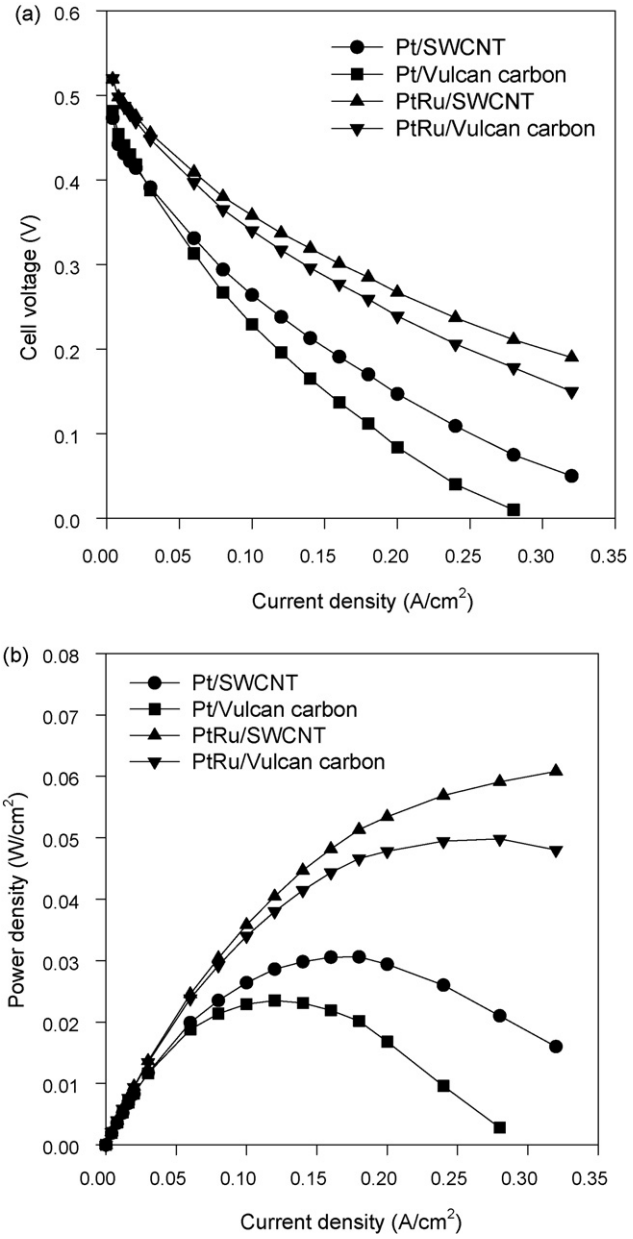

Fig. 9. (a) Polarization curves and (b) output power of single cell at 80 °C. Anode: Pt/SWCNT or Vulcan carbon and PtRu/SWCNT or Vulcan carbon (4 mg cm^{-2}), 2 M CH_3OH 2 ml min^{-1}. Cathode: Pt/C(E-TEK) (3 mg cm^{-2}), O_2 500 cm^3 min^{-1}.

Using the polarization curves for different catalysts (Fig. 8), Tafel plots were obtained from the onset region of the linear polarization curve at high overpotentials. This involved use of the reduced form of the Butler–Volmer equation [34]:

$$\log i = \log i_0 + \left(\frac{\alpha_A n F}{2.303 RT}\right)\eta \quad (2)$$

where η is the overpotential; i_0 the exchange current density; α_A the anodic transfer coefficient; all other symbols have their usual meanings. Two distinct slopes are evident from Tafel plots in Fig. 8. Slopes of 195 and 196 mV per decade are obtained for the Pt/SWCNT and Pt/Vulcan carbon, and the slopes 157 and 154 mV per decade for the PtRu/SWCNT and PtRu/Vulcan carbon. Tafel slopes of 180–195 mV per decade have been reported for methanol oxidation at 60 °C on a PtRu alloy [35], carbon-supported PtRu catalysts [36] and a SWCNT-supported Pt catalyst [18]. Lower values of 110–140 mV per decade have also been found for carbon-supported PtRu catalysts [37–39]. At a potential above 0.6 V for Pt/SWCNT and Pt/Vulcan carbon and above 0.35 V for PtRu/SWCNT and PtRu/Vulcan carbon, the slopes of the E versus $\log I$ line increase and of limiting current is reached. It should be noted that the limiting current is not mass-transfer controlled and it cannot be enhanced by rotating the electrode. This behaviour may be attributed to the formation of a weakly adsorbed intermediate [40,41]. The shift in the onset potential for methanol oxidation suggests that the SWCNT has a major catalytic effect on the surface reactions that are occuring. Britto et al. [42] have shown an improvement in charge transfer at carbon nanotube electrodes.

The current–potential and power density curves of a single DMFC, are given in Fig. 9. The anode of the MEA is supplied with 2 M methanol solution and the counter electrode with O_2 that is pressurised to 0.2 MPa at the same temperature of the cell (80 °C). There is virtually no change in the open-circuit voltage when different catalysts are employed. As found in cyclic voltammetry tests, anodes with PtRu present better performances than those with Pt. Enhanced performance and power density are achieved using the SWCNT support (PtRu/SWCNT better than PtRu/Vulcan carbon, Pt/SWCNT better than Pt/Vulcan carbon). A power density of 50 mW cm^{-2} for a PtRu/SWCNT anode is attained at 80 °C.

4. Conclusions

Pt and PtRu nanoparticles have been formed in an ethylene glycol solution and subsequently transferred to toluene using dodecanethiol as the phase-transfer agent. The Pt and PtRu particles are nanosized and have relatively narrow particle-size distributions. Results obtained from XPS analysis reveal the strong attachment of the sulfur end of thiol to the surface of the metal nanoparticles. The metals are mostly in the reduced form (Pt(0) and Ru(0)), with some traces of Pt(IV) and Ru(IV). The metal colloids are adsorbed on SWCNT or Vulcan carbon and heat treated to remove the dodecanethiol shell. The resulting catalysts are active in the room temperature electrooxidation of methanol. The bimetallic catalysts are more active than the Pt-only catalyst and less receptive to methanolic residue deactivation. PtRu catalysts exhibit lower onset potentials for methanol oxidation. Based electrochemical and fuel cell studies, the PtRu catalyst dispersed on SWCNT exhibits the best performance.

References

[1] S. Wasmus, A. Kuver, J. Electroanal. Chem. 461 (1999) 14.
[2] X. Ren, P. Zelenay, S. Thomas, J. Davey, S. Gottesfeld, J. Power Sources 86 (2000) 11.
[3] J.G. Liu, T.S. Zhao, R. Chen, C.W. Wong, Electrochem. Commun. 7 (2005) 288.
[4] Z.L. Liu, J.Y. Lee, M. Han, W.X. Chen, L.M. Gan, Langmuir 20 (2004) 181.
[5] J. Prabhuran, T.S. Zhao, H. Yang, J. Electroanal. Chem. 578 (2005) 105.
[6] A.G. Fendler, D. Richard, P. Gallezot, Faraday Discuss. 92 (1991) 69.
[7] M. Watanabe, M. Uchida, S. Motoo, J. Electroanal. Chem. 229 (1987) 395.
[8] T.J. Schmidt, M. Noeske, H.A. Gasteiger, R.J. Behm, J. Electrochem. Soc. 145 (1998) 925.
[9] H. Bönnemann, R. Brinkmann, P. Britz, U. Endruschat, R. Mörtel, U.A. Paulus, G.J. Feldmeyer, T.J. Schmidt, H.A. Gasteiger, R.J. Behm, J. New Mater. Electrochem. Syst. 3 (2000) 199.
[10] Z.L. Liu, X.Y. Ling, X. Su, J.Y. Lee, J. Phys. Chem. B 108 (2004) 8234.
[11] E.M. Crabb, R. Marshall, D. Thompsett, J. Electrochem. Soc. 147 (2000) 4440.
[12] J.C. Huang, Z.L. Liu, C.B. He, L.M. Gan, J. Phys. Chem. B 109 (2005) 16644.
[13] M. Götz, H. Wendt, Electrochim. Acta 43 (1998) 3637.
[14] C.A. Bessel, K. Laubernds, N.M. Rodriguez, R.T.K. Baker, J. Phys. Chem. B 105 (2001) 1115.
[15] E.S. Steigerwalt, G.A. Deluga, C.M. Lukehart, J. Phys. Chem. B 106 (2002) 760.
[16] G.L. Che, B.B. Lakshmi, C.R. Martin, E.R. Fisher, Langmuir 15 (1999) 750.
[17] W.Z. Li, C.H. Liang, J.S. Qiu, W.J. Zhou, H.M. Han, Z.B. Wei, G.Q. Sun, Q. Xin, Carbon 40 (2002) 791.
[18] G. Girishkumar, K. Vinodgopal, P.V. Kamat, J. Phys. Chem. B 108 (2004) 19960.
[19] X.G. Li, S.H. Ge, C.L. Hui, I.M. Hsing, Electrochem. Solid State Lett. 7 (2004) A286.
[20] W.Z. Li, C.H. Liang, W.J. Zhou, J.S. Qiu, H.Q. Li, G.Q. Sun, Q. Xin, Carbon 42 (2004) 436.
[21] M. Carmo, V.A. Paganin, J.M. Rosolen, E.R. Gonzalez, J. Power Sources 142 (2005) 169.
[22] G. Girishkumar, T.D. Hall, K. Vinodgopal, P.V. Kamat, J. Phys. Chem. B 110 (2006) 107.
[23] K.W. Park, Y.E. Sung, S. Han, Y. Yun, T. Hyeon, J. Phys. Chem. B 108 (2004) 939.
[24] T. Teranishi, M. Hosoe, T. Tanaka, M. Miyake, J. Phys. Chem. B 103 (1999) 3818.
[25] S.Y. Zhao, S.H. Chen, S.Y. Wang, D.G. Li, H.Y. Ma, Langmuir 18 (2002) 3315.
[26] D.N. Furlong, A. Launikonis, W.H.F. Sesse, L.V. Sanders, J. Chem. Soc. Faraday Trans. 1 80 (1984) 571.
[27] V.I. Pârvulescu, S. Coman, P. Palade, D. Macovei, C.M. Teodorescu, G. Filoti, R. Molina, G. Poncelet, F.E. Wagner, Appl. Surf. Sci. 141 (1999) 164.
[28] N. Toshima, M. Harada, Y. Yamazaki, K. Asakura, J. Phys. Chem. 96 (1992) 9927.
[29] M.M. Maye, W. Zheng, F.L. Leibowitz, N.K. Ly, C.J. Zhong, Langmuir 16 (2000) 490.
[30] C.D. Wagner, et al., Handbook of X-ray Photoelectron Spectroscopy, Perkin-Elmer Corporation, 1979.
[31] M.M. Maye, J. Luo, Y. Lin, M.H. Engelhard, M. Hepel, C.J. Zhong, Langmuir 19 (2003) 125.
[32] R.J. Woods, Electroanal. Chem. 9 (1976) 1.
[33] D. Chu, S. Gilman, J. Electrochem. Soc. 143 (1996) 1685.

[34] A.J. Bard, L.R. Faulkner, Electrochemical Methods. Fundamentals and Applications, 2nd ed., John Wiley & Sons, New York, 2001.
[35] H.A. Gasteiger, N. Markovic, P.N. Ross, E.J. Cairns, J. Electrochem. Soc. 141 (1994) 1795.
[36] T.J. Schmidt, H.A. Gasteiger, R.J. Behm, Electrochem. Commun. 1 (1999) 1.
[37] G. Méli, J.-M. Léger, C. Lamy, R. Durand, J. Appl. Electrochem. 23 (1993) 197.
[38] C. He, H.R. Kunz, J.M. Fenton, J. Electrochem. Soc. 144 (1997) 970.
[39] C. Roth, N. Marty, F. Hahn, J.-M. Léger, C. Lamy, H. Fuess, J. Electrochem. Soc. 149 (2002) E433.
[40] Z. Jusys, J. Kaiser, R.J. Behm, Electrochim. Acta 47 (2002) 3693.
[41] S.L.J. Gojković, T.R. Vidaković, D.R. Durović, Electrochim. Acta 48 (2003) 3607.
[42] P.J. Britto, K.S.V. Santhanam, A. Rubio, J.A. Alonso, P.M. Ajayan, Adv. Mater. 11 (1999) 154.